Bacterial flagellar motor as a multimodal biosensor

Bacterial Flagellar Motor as a Multimodal Biosensor

Ekaterina Krasnopeeva[a], Uriel E. Barboza-Perez[a], Jerko Rosko[b], Teuta Pilizota[a,d], Chien-Jung Lo[c,d]

[a] *Centre for Synthetic and Systems Biology, School of Biological Sciences, The University of Edinburgh, Edinburgh, United Kingdom*
[b] *Laboratoire Jean Perrin, Sorbonne Université, Paris, France*
[c] *Department of Physics and Graduate Institute of Biophysics, National Central University, Jhongli, Taiwan, Republic of China*
[d] *Corresponding authors*

Abstract

Bacterial Flagellar Motor is one of nature's rare rotary molecular machines. It enables bacterial swimming and it is the key part of the bacterial chemotactic network, one of the best studied chemical signalling networks in biology, which enables bacteria to direct its movement in accordance with the chemical environment. The network can sense down to nanomolar concentrations of specific chemicals on the time scale of seconds. Motor's rotational speed is linearly proportional to the electrochemical gradients of either proton or sodium driving ions, while its direction is regulated by the chemotactic network. Recently, it has been discovered that motor is also a mechanosensor. Given these properties, we discuss the motor's potential to serve as a multifunctional biosensor and a tool for characterising and studying the external environment, the bacterial physiology itself and single molecular motor biophysics.

Keywords: bacterial flagellar motor, Proton Motive Force, chemotaxis, mechanosensing, biosensor, bacterial physiology, single molecular biophysics

Bacterial flagellar motor's sensing potential

Bacterial flagellar motor (BFM) is a unique example of a rotary molecular machine that has captivated scientists for several decades [1, 2, 3, 4, 5]. The knowledge gained now opens the possibility of using the motor for sensing of multiple variables of interest. The evolutionary function of the motor is to

enable propulsion of several bacterial species via rotating either a single flagellum (*Vibrio alginolyticus*, *Caulobacter crescentus*) or a bundle of flagellar filaments (*Escherichia coli*, *Salmonella typhimurium*, *Bacillus subtilis*) [1, 6], at the base of which is the BFM. Multiple reviews focus on the BFM's structure and function [3, 4, 7] as well as give a summary of the experimental and theoretical milestones achieved while studying the motor [5], and we direct the reader to those for details. Here, we summarise BFM's main features focusing on the aspects that are most relevant for its use as a biosensor.

The BFM consists of several concentric protein rings that span the cross-section of the entire cell envelope, composed of one or two cell membranes (for the case of gram-positive and gram-negative bacteria, respectively) and a stiffer cell wall, Fig.1. Like a macroscopic motor, the BFM has a rotor and a stator. The rotor consists of the cytoplasmic (C) and the membranous/supramembranous (M, S) rings. Its rotation is driven by the stator, consisting of a varying number of MotA/MotB units (or PomA/PomB, depending on whether the motor is driven by proton or sodium ions, respectively) [8, 9, 10, 11, 12]. Every stator unit has been thought to consist of 4 MotA and 2 MotB proteins, however recent crystal structures show this to be 5 MotA and 2 MotB subunits, as shown in Fig. 1 and Fig. 5A [13, 14]. The torque generated by the stator is powered by the energy released upon the transit of ions across the cellular membrane (so called Ion Motive Force-IMF), reaching as high as few thousands pN·nm [4]. The BFM's rotational speed can reach up to a couple of thousand rotations per second [15] and it is proportional to the IMF. The number of torque-generating units incorporated in the stator at a given time point depends on the motor's torque. Thus, changing either the IMF or the applied load on the motor results in stator unit engagement or disengagement [10, 11, 12]. The rotational direction of the motor is controlled by the chemotactic network [16, 17, 18], enabling the cell to divert its movement in the chemical concentration gradients of attractant or repellent molecules [19]. Given these properties, measuring the motor's speed and rotational direction offers information on both IMFs and the external environment, and we next discuss the experimental tools needed to achieve it. We subsequently give examples of employing the motor for different sensing modalities, and finally, we discuss future directions, including the limitations of using the BFM as a biosensor.

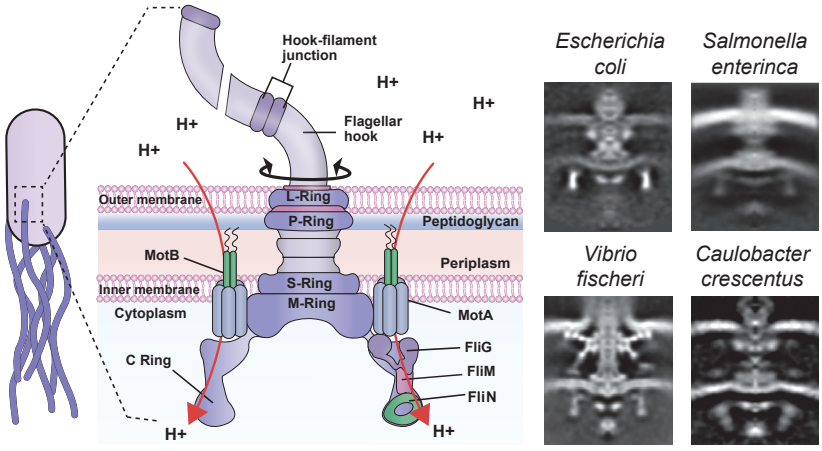

Figure 1: Bacterial flagellar motor. Rotor consists of M, S and C rings. The latter is a stack of multiple copies of FliG, FliM, FliN proteins, each arranged in a ring, and referred to as the "switch complex" because of involvement in determining the rotational direction of the motor via the FliG-MotA interaction. MotA is a part of the torque generating $MotA_5MotB_2$ units, where MotB subunits anchor the stator to the cell wall (peptidoglycan layer). Rotation of the motor is powered by the ion (in this case, proton) flux through the stator units. The figure and caption are inspired by [20] and [4]. Right panel is taken from EMBL-EBI Protein Data Bank in Europe and shows EM images of BFM from various motile species. While differences between different motors are visible, the EM images also highlight that the main features of rotor/stator arrangement are conserved.

1. Bacterial Flagellar Motor speed and bias measurements

1.1. Free swimming cells

Because the relationship between the swimming speed of a bacterium and the rotational frequency of flagellar filaments driven by the motor has been shown to be roughly linear [21, 22], the changes in BFM speed and direction can be, in principle, estimated from free swimming bacteria, Fig. 2A.

Bacteria are micron-scale organisms, usually swimming with speeds varying between tens and hundreds of body lengths per second [23, 24, 25, 26], and thus, tracking them to measure their swimming velocity is not a trivial task. The efforts to do so can be broadly divided into measuring the single bacterium run speeds and tumbling rates [23, 27, 24, 28, 29][30, 31], and measuring the average speed of a bacterial population [32, 33].

The first successful tracking of a single bacterium in 3D was performed by Howard Berg in 1971 [23]. In his setup, a custom built sample chamber compensated for the movements of the cell of interest, so that it stayed

constantly in focus: "The scene through the binocular is extraordinary. The bacterium being tracked seems to be stuck to the center of the field, turning this way and that trying to free itself, while the other bacteria drift in and out of focus, then to and from, in apparent synchrony" [23]. While the view is extraordinary, the method can only track single bacterium at a time, and it requires a complex setup with a sample chamber capable of rapid movements in three dimensions [23, 29]. With the progress of imaging technology new approaches were implemented for both 2D [34, 24] and 3D [28, 35] tracking. Although 3D tracking requires more complex analysis, such as machine learning algorithms [35] or image cross-correlations between the observed diffraction patterns and a reference library [28], it also gives more accurate information of the cell movements when compared to 2D methods, which work either with projections [34] or with selected short trajectories that lay within the narrow band of the image depth [24]. With recorded single cell trajectories, that represent a random walk with intervals of run and tumble [36], the speed can be measured for the run intervals and the tumbling rate calculated as the number of turns divided by the duration of the trajectory [29]. Here, tumbles are usually defined based on a set change in angle between subsequent cell body directions [28].

Alternative to the single cell tracking is the analysis of large populations, e.g. differential dynamic microscopy (DDM), which allows measurements of the speed distribution of over 10^4 free swimming cells [32, 33]. It works by recording low magnification videos of swimming bacteria and analysing the statistics of temporal fluctuations of pixel intensities, which are caused by the variation in the density of bacteria. It measures the differential image correlation function (DICF), which is effectively a power spectrum of the difference between two images taken at separate time points [32, 33]. Although the method does not require a complex physical setup, it relies on the knowledge of the underlying process that generates the specific DICF, to which the data is fitted [32, 33] (e.g. obtaining swimming speeds is easier than obtaining the run duration because of the broad range of relevant length and time scales involved in the latter [37]).

An advantage of using swimming velocity to gain information on BMF's rotation is the ease of sample preparation. Bacteria are grown, introduced into an imaging chamber and immediately observed. However, because swimming bacteria move freely in 3D or 2D environment it is not possible to exchange the external medium during the measurements, and with population measurements it is also not possible to access cell to cell heterogeneity, which

could play a role in successful employment of biosensors [38].

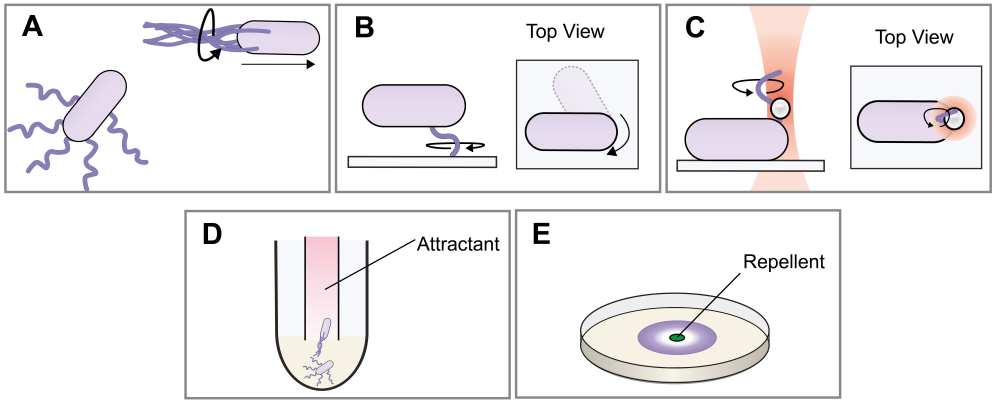

Figure 2: Bacterial flagellar motor speed and bias measurements: **A.** Free swimming bacteria are shown in running and tumbling modes [23, 24, 27, 28, 29, 32, 33]; **B.** Tethered cell (side and top view) is anchored to the surface via flagellum and is capable of rotating around the attachment point [2, 39, 40, 41, 42, 43, 44, 45]; **C.** Bead assay (side and top view) uses a plastic bead attached to the "sticky" flagellum whose rotational speed is measured with back-focal-plane interferometry [46, 47]. The method relies on a sharply focused but heavily attenuated laser that records the bead trajectory as an interference patter projected to a position sensitive detector [4, 5, 48, 49, 50, 51, 52]. **D** and **E** show chemotaxis assays: **D.** Capillary method where accumulation of bacteria in the capillary filled with chemical solution show the level of attraction/repulsion [53, 54]; and **E.** soft agar swimming plate allows observation of cell density distribution as a function of distance from the repellent/attractant source [55]

1.2. Tethered cells

Tethered cells, Fig. 2B, were first used to confirm that flagella move in a rotary motion, rather than by a propagation of the helical waves [1, 2]. In the experiment performed by Michael Silverman and Melvin Simon in 1974, cells were attached to a cover glass by a flagellum via the antipolyhook antibody. The motor-driven rotation of the cell body relative to the attachment point is one of the most striking demonstrations of the action of a molecular motor [2]. Later, it became possible to use the "sticky" flagella phenotype instead of antibodies to attach cells to the glass. The phenotype was obtained in 1988 as a by-product of experiments aimed at acquiring a minimum-size functional flagellum, where a $\sim$50 amino acids mutation to the single protein of which the flagellum is composed, significantly changed its hydrophobicity

[56]. Tethered cell technique proved to be easy, reliable and thus has been widely used over time to investigate the BFM's torque generating mechanism [39], mechanosensing [40, 41], chemotaxis [42] or as a qualitative indicator of the PMF or membrane voltage change [43, 44, 45].

Because the cell body imposes a large load on the motor, the rotational speed usually stays below 10 Hz (unless external torque is applied) [2, 45, 43], which is easily detectable by cameras with frame rates exceeding 30 fps. The preparation of cell culture for the tethered cell experiment is quite straightforward as the hydrophobic "sticky" flagella do not require any chemical pre-treatment for attachment to glass. However, the method does not allow the control of the attachment geometry nor the load itself, as cell size varies in a population. Consequently, this technique reports large spread of rotational speeds seen, for example, in [57].

1.3. Single motor bead assay

To obtain higher rotational speeds and gain better control of the load on the motor, it has been suggested to use micron-sized particles (beads) as markers for motor rotation [2]. The breakthrough was the "sticky" filament phenotype that not only enabled spontaneous sticking of filaments to the cover glass, but also to commercially available polystyrene beads that come in various, tightly controlled sizes starting as low as 0.2 μm in diameter [58, 48]. If the filament is shortened ("sheared") to a stub, the load on the motor is by and large imposed by the bead, which rendered the bead assay into a well established tool for studying individual BFMs [4, 5, 48, 49, 50, 51, 52].

To achieve even lower loads for studies of BFM mechanism, the bead assay was modified to include nanometer-sized gold particles (beads or rods) [59, 58]. Given the nm-size of the load, such studies are performed in strain backgrounds that lack the filament protein encoding gene, and the beads are instead attached to the motor hook, a 50 nm in size structure that acts as a universal joint, but can be genetically modified to be longer and more rigid [59, 58, 60]. The attachment is achieved either using antipolyhook antibody [59, 58], streptavidin-biotin link or a cystein introducing mutation [61, 12, 60]. Depending on the viscous load, motor rotation frequency can vary from dozens to hundreds of Hz [4] and can be measured with high speed cameras [12], or back-focal-plane interferometry, where the rotating bead is placed in the focus of a heavily attenuated laser beam and the changes in the interference pattern are recorded with the quadrant photo-diode or position sensitive detector, Fig. 2C [11, 62, 58, 63, 52, 64]. Back-focal-plane

interferometry provides high temporal resolution (up to 0.5 ms [65] and the limit is set by the particle drag rather then the sampling rate of the position sensitive detectors or diodes), allowing precise motor speed and rotational direction measurements. In addition, the technique can easily be combined with parallel fluorescence imaging [52, 64]. However, the method requires an optical trap setup and can only target a single motor per experiment [48, 58, 52]. Furthermore, the sample preparation proceeds in a series of steps, e.g. filament shearing, attachment of cells to the surface and attachment of beads to the cell filaments or hooks [58, 52, 62], which further lowers the throughput.

Alternative methods of motor driven bead rotation detection have recently been looked at, such as an impedance-based electronic detection [66, 67]. Although the signal-to-noise ratio is currently poor [67], this is a promising field of research that can result in a device detecting multiple individual motors at the same time. Because the output is in an electronic form, the method can become a game changer, enabling portable biosensor-on-the-chip configuration of motor speed and rotational direction detection.

1.4. Chemotaxis assays

Bacterial chemotaxis can be studied without direct observation of the motor's rotation. For example, at the end of 19^{th} century Wilhelm Pfeffer developed a method that consisted of a capillary tube filled with a solution of some chemical of interest, and a "pond" of bacteria [53, 16]. The tube was inserted into bacterial suspension and the accumulation of bacteria inside, or away, from the capillary was observed, Fig. 2D. The technique, later adapted by Julius Adler, is commonly known as the "capillary method" and was used in a series of experiments studying chemotaxis [68, 54].

Another common technique for studying chemotaxis, termed the "chemical-in-plug method", uses plates with soft agar where bacteria can swim and accumulate next to the source of chemical attractant or away from the repellent, Fig. 2E. The attractant or repellent gradient is created by diffusion from a hard agar plug containing the a chemical of interest, which is inserted into the soft agar [55].

While these methods provide mostly qualitative description of the chemotaxis, they may still be useful for identifying the presence of attractant or repellent molecules in the environment and could be exploited in biosensing assays for detection of very low concentrations of the substance of interest.

2. Harnessing the Bacterial Flagellar Motor sensing capabilities

2.1. BFM as a chemosensor

The ability of bacteria to move towards nutrients and away from harmful chemicals was first noticed over a 100 years ago and has been extensively studied after [69, 53, 70]. As an example of chemotactic system at work, let us consider *E. coli*. Each bacterium has about half a dozen bacterial filaments distributed along the cell body. The filaments can form a bundle at the back of the cell when all of the BFMs rotate counterclockwise (CCW), thus allowing the cell to swim in a roughly straight line (or in a clockwise circular motion near solid surfaces) [1, 71, 72, 3]. In the absence of chemical signals in the environment, every couple of seconds, one, or most likely, a few motors switch to clockwise rotational direction (CW) and their respective filaments fall out of the bundle, leading to a tumble [73, 74]. Forward swimming (likely in a different direction due to approximately random reorientation of the bacterial cell during the tumble event) resumes when motors switch back to the CCW direction and the bundle reforms [1, 73]. Thus, without chemical signals *E. coli* performs a random walk. In the presence of chemical signals in the environment, the probability of a motor switch to CW direction either decreases or increase, depending on whether the chemical signal is an attractant or repellent[17, 19], resulting in biased random walk toward or away attractants or repellents, respectively [17, 18].

The switch to CW rotation is initiated with the interaction of the phosphorylated CheY protein (CheY-P) with the motor switch complex [75, 76, 77], Fig. 3A. In such a way, CheY plays a key role in chemotactic signal transduction from the transmembrane chemoreceptors called Methyl-accepting Chemotaxis Proteins (MCPs) to the BFM [78, 79]. The MCPs span the inner membrane and the periplasmic space between the two membranes to extend into the cytoplasmic space, and thus transmit the information on the presence of specific chemicals in the extracellular environment [80, 74]. The MCPs can sense very low concentrations of specific chemicals, usually in the tens of nanomolar to tens of micromolar range [16]. For higher concentrations the signal saturates [81, 82], and for concentrations that can cause significant osmolarity changes the motor's response involves both speed increase and rotational direction changes [62].

The sensing is specific to a set of chemoeffectors (attractants or repellents), where attractants have been more extensively studied, and include molecules such as sugars, amino acids and quorum sensing molecules [83, 84,

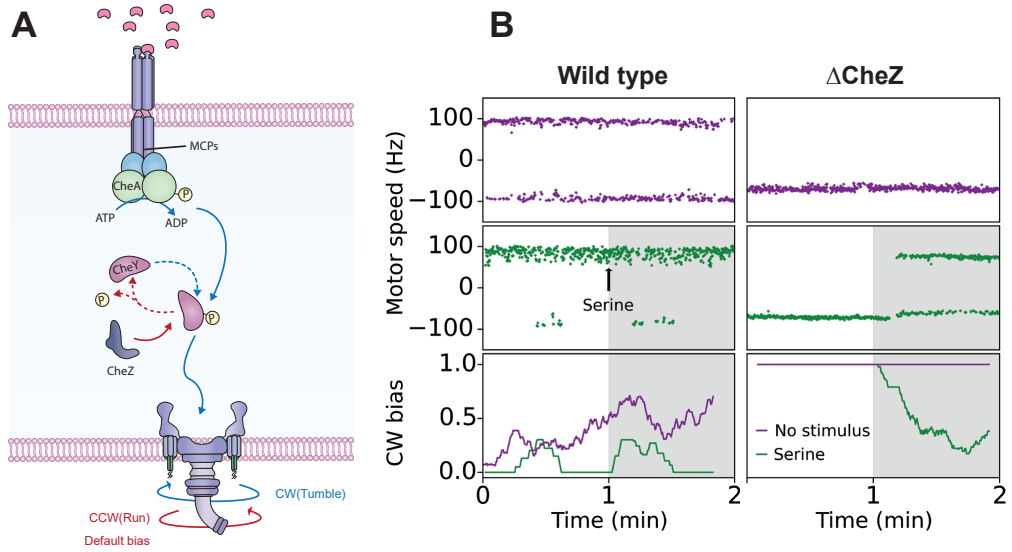

Figure 3: Use of the BFM as a chemosensor. **A.** A schematic of the chemotactic network. MCPs protrude cell envelope and detect external stimulus by binding chemoeffector molecules and activating CheA kinase. Activated CheA phosphorylates signal protein CheY. CheY-P interacts with the switch complex of the BFM changing its rotational direction from CCW to CW. The system is reset when CheZ phosphatase removes phosphoryl group of CheY-P and motor resumes CCW rotation. **B.** An example of motor speed recordings with chemotactic stimulus for a wild type *E. coli* and a ΔCheZ strains. *Top panel* shows the motor rotation of a wild type chemotactic strain with attractant (serine) introduced at 1 min time point (shaded grey area). Positive frequencies correlate to the CCW and negative to the CW motor rotation. *Middle panel* shows the same for the ΔCheZ mutant strain. With no chemical stimulus the motor predominantly rotates CW, as CheY-P dephosphorylation is $\sim$ 100 times slower without CheZ. After addition of serine (grey area) the motor starts rotating CCW, as CheY phosphorylation is now inhibited. *Bottom panel* shows the comparison of CW Biases for the two strains: purple for WT and solid green for ΔCheZ mutant. Transparent green lines show biases of the mutant strain in three more repeats of the experiments. While wild type rotation pattern hardly changes on the detectable time scales, while ΔCheZ mutant motor Bias decreases significantly in the presence of an attractant.

85, 86]. Repellents are relatively less well studied, and include molecules such as metal ions (Co^{2+}, Ni^{2+}), acetate and indole [55, 87], leaving the possibility that some of the MCPs-specific repellents are yet to be identified. Additionally, recent studies have shown that it is possible to create functional hybrid receptors by fusing sensory domains from other species [88, 89, 90], and syn-

thetic receptors with single-domain antibodies as sensing domains [91, 92]. These modifications can boost the sensing range and improve the response times. The signals detected by the MCPs travels down the network to the motor on the time scales of seconds, and the response of the motor lasts only a few seconds before being reset to the initial state [93]. Specifically, CheY is phosphorylated by activated CheA kinase [79, 94], and has a natural auto dephosphorylation rate of $\sim 8.5 \times 10^{-2}$ s^{-1} [95], with a half-life time of 14-20 s [96, 74]. However, in *E.coli* CheY dephosphorylation is actively performed by phosphatase CheZ, accelerating the reset time by a factor of $\sim$100 [97, 74] and allowing continuous sensing in a chemical gradients. To utilise the BFM as a chemical sensor, the duration of the change in motor's rotational direction should be extended. In Fig. 3B we show the response of a genetically modified strain to fit the purpose. The strain lacks CheZ and thus in the environment with no specific MCPs binding chemicals shows almost exclusively CW Bias (defined as N_{CW}/N_{tot}, where N_{CW} is the time spent rotating in CW direction and N_{tot} the total time spent rotating in either direction), Fig. 3B. Upon addition of an attractant CW Bias decreases for an extended period of over 60 s making it easier to detect the change. To sense repellents, ΔCheZ mutant should be complemented with a plasmid carrying CheZ so that the steady-state CW Bias is tuned to desired lower values while preserving the longer response time. Furthermore, most, if not all, reported whole-cell biosensors, which currently predominantly use expression of a fluorescent protein as the output [98, 99, 100, 101, 102], can be modified to use BFM's CW Bias instead. To do so, instead of a fluorescent protein the sensor should express a genetically modified CheY protein that mimics the CheY-P form (so called CheY** [103]). Altering the output of the whole-cell sensors from fluorescent proteins to CW Bias extends the range of detection techniques, e.g. those described in Section 1 or discussed in Summary.

2.2. BFM as a voltmeter

Because BFM's rotation is powered by the IMF [104, 3] and the relationship between the motor speed and the IMF is linear [57, 45], the motor can be used as a sensor for single-cell electrophysiology [52]. In case of *E. coli* or *Salmonella*, the driving ions are protons and the BFM is powered by the Proton Motive Force (PMF), Fig. 1. In *Vibrio* species the motor is put in motion with the flux of sodium, so-called Sodium Motive Force (SMF) [58]. Here, we will consider a use of proton-driven *E. coli* motors as an equivalent of a single-cell voltmeter.

Given that PMF is an electrochemical potential of protons it defines the amount of the potential energy required to pump a proton up its gradient. It is related to other proton potentials as $PMF = V_m - \frac{2.3RT}{F}\Delta pH$ [105], where V_m is membrane voltage and ΔpH the difference between internal and external pH, R is the gas constant, T the temperature and F Faraday constant. The PMF is a result of the electron transport chain activity and a key intermediate in biological energy conversion. It's employed in multiple processes occurring on the bacterial membrane such as ATP synthesis, ion transport and bacterial motility [105, 106, 39, 57].

In 1995 David Fung and Howard Berg demonstrated for the first time that the BFM's frequency varies linearly with the PMF [57]. In this work filamentous *E. coli* cells (grown in the presence of cephalexin) were held with the micropipette, to which an external voltage was applied. Cell's own PMF was collapsed with the ionophore gramicidin S. The motor speed was measured by recording the rotation of the fluorescent marker (a smaller cell attached to the hook of the flagellar motor), and found to be proportional to the applied voltage [57].

The proportionality was subsequently generalised for the motors rotating under different loads in the follow-up paper by Christopher Gabel and Howard Berg [45]. The work compared rotational frequencies of the two motors on the same cell under different external loads, and found that when the cell is treated with the protonophore carbonylcyanide m-chlorophenylhydrazone (CCCP) or the respiratory chain inhibitor sodium azide, the two speeds decrease in a linearly dependent manner. As the speed of the slower motor (under higher load) was proportional to the PMF in an earlier experiment, Gabel and Berg's experiment provided evidence that the linear relationship between motor speed and PMF is not dependant on the load, although the slope of that linear dependency does depend on it. Thus, as long as the load on an individual motor is kept fixed during the experiment the speed-PMF proportionality constant will remain the same.

If the speed of a bacterial flagellar motor can serve as a proxy for the relative change in PMF (for discussion on absolute PMF measurements see Section 3) and, in the environments where $\mathrm{pH}_{external} \sim \mathrm{pH}_{internal}$, in V_m as well [52], one can employ the motor as a sensor of cells' own electrophysiology. Because bacteria are small and electrochemical ion gradients are hard to measure [64, 107], the electrical aspects of cellular behaviour in bacteria have been rarely studied [108, 109]. Yet, the ability to do so would open a range of currently inaccessible questions, which are at the basis of bacterial

free energy maintenance, and consequently, survival. For example, in [52] we combine V_m and PMF measurements with and electric circuit analogy of an *E. coli* cell to infer the mechanism and dynamics of the damage as the cells are exposed to several chosen external stresses. Fig. 4 shows results obtained under butanol treatment. PMF sharply drops upon butanol addition, the drop magnitude depends on the butanol concentration and PMF quickly recovers after butanol removal. The behaviour is characteristic of a ionophore, and we were able to determine the functional dependency of overall membrane resistance under different butanol concentrations.

Apart from PMF, BFM speed can also be used to assess SMF because sodium stator units from *V. alginolyticus* can be expressed in *E. coli* (so called chimeric motor) [110, 111]. Furthermore, in the absence of Na^+, *V. alginolyticus* motor can be driven by Li^+ [112], and alkaliphilic bacterium *Bacillus alcalophilus* motor has been found specific to Na^+, K^+ and Rb^+ [113], opening the possibility of using the motor as a sensor for a range of electrochemical gradients.

2.3. BFM as a mechanosensor

An additional property of the BFM that could be employed for sensing purposes is its ability to remodel under different torque. While discovered only recently, hints of mechanosensing have been noticed three decades ago. For example, Steven Block and Howard Berg noticed that stator units can be successively incorporated into the motor, an event observed via a characteristic step-wise increase in the rotational speed [114]. Since, it has been discovered that the number of stator units can reach up to at least 11 [9], and that a single stator unit remains bound to the rotor, on average, 30 s before returning to a membrane pool of $\sim$100 units [40]. Finally, in 2013 the motor was shown to dynamically change the number of stator units in response to a change in the external load, or the motor speed, which proved definitively that the BFM is able to mechanosense, Fig. 5A and [11, 10].

The kinetics of arrival and departure of the stator units have been studied using rotating magnetic or electric fields that enable application of an external torque on the motor [12, 41]. Based on these experiments it has been reported that the mechanism behind mechanosensing is a catch-bond, in which the dissociation rate of stator units increases with decreased motor torque [12]. Fig. 5B shows an example of normalised motor speed trace after the motor has been externally stalled for 5 min. The increase in speed after

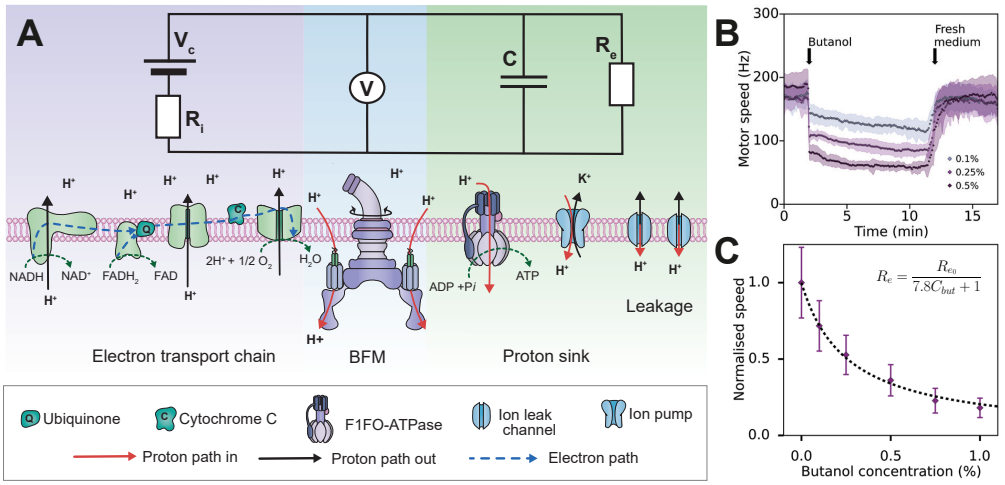

Figure 4: Use of the BFM as a single cell voltmeter. **A.** Cell is represented as an electric circuit. Here, the respiration complex plays the role of the imperfect battery V_c with an internal resistance R_i. The battery is the theoretical maximum voltage that can be obtained from a given carbon source once it is internalised, and R_i is the loss from that maximum due to metabolism. The membrane with different ion proteins (antiporters, symporters, channels, etc.) functions as an external resistance and a capacitance connected in parallel. In the absence of ΔpH BFM can be used as a membrane voltage indicator, i.e. a single cell voltmeter [52]. **B** and **C** show how measurements of relative PMF changes can enable determining the effects of an external stress (butanol) on *E. coli* [52]. **B.** Mean speed with standard deviation traces for cells treated with 0.1, 0.25 and 0.5% butanol. Butanol is added to the cells at 2 min time point and removed at 12 min. The motor speed drops sharply upon butanol addition but reverses to the initial value after its removal. **C.** Mean speeds after the butanol shock are calculated and normalised to the initial speed and plotted with standard deviation against butanol concentration. Black dotted line is a hyperbolic fit. Using this fit in combination with circuit analogy of a bacterium allowed us to show that butanol changes permeability of the membrane in an ionophor-like manner with the concentration dependency shown in **C** [52].

the motor release demonstrates additional stator units are recruited during the stall [12].

The biological role of mechanosensing is not yet understood, although it has been proposed to be involved in swimming in changing environments and in surface sensing [115, 116, 117]. Recent preliminary results reported in [51] suggest that the motor is capable of sensing shear stress imposed on the motor by a transient change in the fluid flow, Fig. 5C. In the experiment, cells attached to the surface experienced a manually administered 10-15 s long pulse of flow, where the local flow velocity was on the order of ∼1000 µm/s,

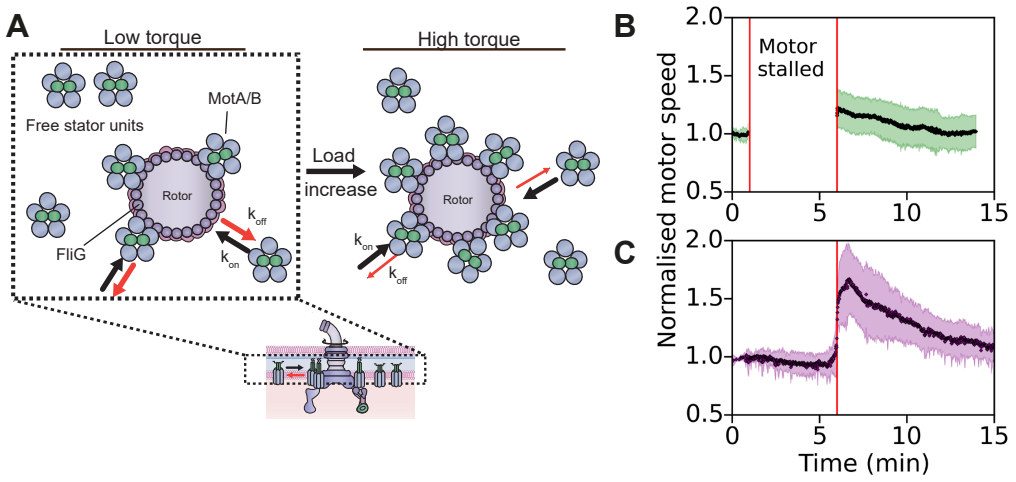

Figure 5: Use of the BFM as a mechanosensor. **A.** An illustration of motor remodelling upon the torque change. Top view of the rotor with a number of bound stator units is shown on the left. Free stator units floating in the membrane associate to the motor with the rate defined by k_{on}, which in steady state is equal to the bound units dissociation rate k_{off}. When the torque changes, e.g. increases due to the viscous load increase, k_{off} decreases resulting in the higher number of stator units bound to the motor. **B.** An example of mechanosensing shown in [12]. The motor with 0.5 μm magnetic bead attached to it is stalled by the external magnetic field for 5 min, increasing the load to maximum. Speed immediately after motor release is 20-30% higher than the initial value. However, the speed recovers to the initial value within several minutes. The mean speed normalised to the speed before stall with standard deviation is plotted for 40 motors. Data is kindly provided by Ashley Nord [12]. **C.** Shear flow sensing experiment from [51]. *E. coli* cells attached to the cover glass are subjected to manually administered rapid flow (local flow velocity on the order of ∼1000 µm/s) for 10-15 s (indicated by the red line). Black line shows the mean speed value of 14 motors, with standard deviation shown in purple shading. Upon flow cessation, speed increase of 50-100% is observed, and the speed recovery kinetics is not unlike that in **B**.

resulting in a short-term 40-60% increase in the motor speed, followed by relaxation to the initial value. Kinetics of the speed change appear similar to the previously reported speed changes characteristic for mechanosensing due to load change [12]. While the role of shear sensing remains to be discovered, if further characterised, the result opens the possibility of using the BFM as a flow biosensor.

Furthermore, surface sensing has been shown to trigger a BFM-mediated genetic response in *Vibrio*, *Caulobacter*, and *Bacillus* species as well as in pathogenic *E. coli* [118, 119, 120, 121]. These results could be used for creat-

ing a biological mechanosensor with fluorescent or other genetically encoded output.

3. Limits of BFM usage as biosensor

3.1. Growth conditions and bacterial strains

To use the motor as a sensor the correct strains and growth conditions need to be selected to maximise the yield. Firstly, expression of flagellar genes is inhibited in *E. coli* strains lacking insertion sequence (IS*1* or IS*5*) in the regulatory region of the *flhD* promoter [122]. To use the motor as a biosensor these sequences should be inserted in the desired background to decrease the transcription inhibition level [123]. Furthermore, Julius Adler noticed as early as 1960s that *E. coli* motility varies with growth condition, peaking in post-exponential phase and declining in stationary [124, 125, 126]. However, recent experiments show that the observation was likely made based on the value of optical density of the culture, rather than the number of generations cells divide from an overnight culture before running out of a component of the growth media [123]. When *E. coli* was allowed to divide sufficient number of times in a given growth medium, flagellar genes were expressed in a range of different media, in the exponential phase [123]. However, there are still conditions under which expression of flagellar genes is inhibited and flagellar motor can't be used as a sensor, such as entry into stationary phase [124, 126, 123], surface attachment [127, 128] or exposure to alkaline environment [129].

While the motor speed is proportional to IMF, it can be actively slowed down, e.g. YcgR protein binds to stator units in response to nutrient deficiency and over the course of hours [130, 127]. Thus, for prolonged measurements YcgR deletion background may be required for biosensing purposes. The possibility of an alternative, yet to be identified, mechanism of active speed control should also be kept in mind for each novel condition.

3.2. Stator units dynamics and speed-IMF proportionality

Sensing of electrochemical gradients relies on the linear relationship with the motor speed. For the case of PMF, the proportionality was measured for the -75 to -150 mV range [57], whereas the PMF in *E. coli* can reach as high as $\sim$ -230 mV [131, 132], well beyond the tested range. It is possible that at the higher PMF and under high viscous load, BFM may hit the limit of its maximum torque and thus the limit above which motor speed no longer

changes with PMF. Similar was observed in *V. alginolyticus*, where the BFM speed saturates at the high sodium concentrations (high SMF) in a load-dependent manner [133]. Authors attribute this effect to the limited rate of the sodium association and dissociation kinetics, which may or may not be the case for the proton-driven motor and requires further investigation.

It is worth highlighting that the proportionality between the motor speed and PMF holds despite the fact that the motor is a mechanosensor. As the PMF changes so does the speed, and consequently the torque on the motor as well, which means the number of stator units will change [134, 11, 10]. Yet, all of this happens while maintaining the linear relationship between the speed and the PMF [57, 45], and how is still an open question.

3.3. Calibration

The change in the motor speed can be an indication of PMF, torque or flow variation. However, it only allows one to follow the relative changes in PMF. To have an absolute measure, the speed at a given viscous load has to be calibrated against the PMF. While the emergence of ratiometric, protein based pH sensors, makes the measurements of ΔpH relatively straightforward [52], estimating V_m in gram-negative bacteria may present a challenge [64]. As a potential solution to the problem, one could reduce cell's PMF to only its ΔpH component by collapsing the membrane potential exclusively (e.g. with Valinomycin in the presence of K^+ [135]). Then, the motor rotation will be driven only by the pH difference, which can be measured [52] and converted to mV. The speed calibration must be done for each viscous load. Alternatively, it is possible to calibrate the torque against the PMF.

3.4. Chemotaxis and CW-CCW speed asymmetry

If chemotactically-intact strain is used for the motor speed measurements it is important to consider the speed asymmetry between CW and CCW rotation, Fig. 6 [51]. In 2010, while studying the generation of torque by the motor, Yuan *et al.* reported that the characteristic curves for the relationship between the motor torque and speed were different for CW and CCW rotational directions [136]. For motors rotating faster then 60 Hz, CW direction was slower then CCW [136]. Additional demonstration of CW-CCW speed asymmetry came from the work on chimeric motors in *E. coli* [137]. While no asymmetry has been found in elementary processes, e.g. rotational steps, for CW and CCW rotation [138, 20], the CW speed has been consistently measured slower than the CCW above 60-75 Hz [136, 51]. Thus, for the speed

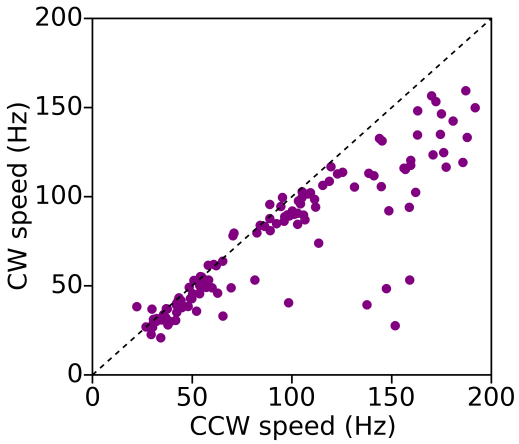

Figure 6: Motors speed in clockwise direction is lower than the counter-clockwise for higher speed values. The full spectrum of motor speeds was obtained by using various PMF and load regimes obtained with different buffers and 1 µm or 0.5 µm beads as the loads. The version of the figure with the conditions resolved in different colours and the list of buffers are available in [51]. Dashed line shows the case where CCW and CW speeds are equivalent (x=y).

measurements it is recommended to use chemotactic mutant strains lacking the ability to rotate CW. Alternatively, at the high motor speeds (above 60-75 Hz) one can use only the positive frequencies when analysing changes in PMF, as the linearity between speed and PMF has been demonstrated for CCW rotation [57].

3.5. Interference of multiple inputs

While BFM is capable of sensing several inputs, the outputs are just two, the rotational speed and the CW Bias. Thus, the possibility of signal interference should be carefully considered for each specific sensing application. When using the motor as V_m/PMF sensor, the load on the motor must be kept fixed during the experiment (sensing), and cells should be kept under controlled and carefully selected environment [52]. For example, to identify the mechanism of action of a given stress, only the concentration/amount of the stress of interest should be altered, and the media of choice otherwise kept unchanged [52]. When sensing specific chemicals, in addition to CW Bias the motor could also change the speed, and the presence of more then one chemical in the environment can result in specificity issues. However, at

the relevant concentrations (nM to μM) we expect any speed changes to be small, and as long as the CW Bias response does not change as the speed does, not relevant for chemical sensing purposes. Furthermore, if the BFM based chemical sensor is designed from whole-cell biosensors, such as those previously published [98, 99, 100, 101, 102], where only the standard GFP output is replaced by the CheY** as discussed earlier, the sensors will remain specific to just one chemical. When relying on the sensing via MCPs in the presence of several repellents, BFM will most likely not be able to distinguish between them. In such a case, the motor can either be used to detect an overall presence of any one of the repellents, or the MCPs need to be engineered for greater specificity, similar to some ongoing efforts [88, 89, 90, 91, 92]. Lastly, the external environment in which the sensor could be deployed in real world can be more complex, so that the steady-state CW Bias is different to the usual (minimal buffer) laboratory conditions [4] even when no repellents are present, and similarly to what was observed in media of higher osmolarities [62]. However, we do not expect that this steady state change will be sufficiently different to mask the response to repellents, and alternatively, the sensor could be primed to the expected composition of the environment to establish the steady-state CW Bias prior stimuli. When sensing the shear flow, it is possible that the chemical composition of the environment will change with the flow, and this could influence the motor speed. The most likely environments where we envision sensing flow are the oceans and rivers, where we expect to sense local changes in flow in otherwise well mixed environments.

Summary

Bacterial flagellar motor has been studied for several decades revealing an interesting set of properties that render it amenable to a number of applications. It is effectively a molecular Swiss army knife that can be used as a non-invasive single cell voltmeter, a mechanosensor for a viscous load or flow detection, and a chemosensor allowing detection of nanomolar concentrations of a specific substance. The sensor's response time and sensitivity can be up to seconds and down to nM concentrations, where the relevant output for a given sensing modality is either the motor's rotational speed or CW Bias. Currently, the available techniques to measure individual motor speed and direction, while high in spatio-temporal resolution, are still relatively low in throughput. However, efforts to detect the rotation of each motor electrically are under way and offer the possibility of multiplexing the task towards a

bio-chip configuration.

Methods

Strain construction and growth. E. coli strain EK07 was used for experiments presented in Fig. 3 [52]. ΔCheZ mutant was obtained by P1 transduction of the CheZ::Kan cassette from JW1870 [139] (The Coli Genetic Stock Center) into EK07 as described previously [140, 141]. For the experiments cells are grown in Lysogeny broth from the frozen stock with 10^3 dilution (for ΔCheZ strain LB is supplemented with 50 μg/ml Kanamycin) at 37°C with shaking (220 rpm) to OD 2.0 (Spectronic 200E Spectrophotometers, Thermo Fisher Scientific, UK) as before [52]. Cells are "sheared" and washed (3 times by centrifugation for 2 min at 8000g) into minimal medium (MM9) pH 7.5 [62, 52]. Tunnel-slides are prepared as in [62, 52].

Motor speed measurements. Motor speed measurements are performed with "bead assay" via back-focal-plane interferometry as before [62, 52]. Chemotactic stimulus is applied as follows: after recording the motor speed for 1 min, 20 μl of MM9 supplemented with L-serine (1 mM) is flushed into the tunnel-slide. Flushing is done by placing the droplet of liquid to one end of the tunnel slide, and immediately collecting it on the other side with a piece of tissue [142]. The flow duration is no longer than 10 s. After the flush, motor speed is recorded for an additional minute without interruption.

Data Analysis. Time series of X and Y coordinates (in Volts) of the bead position are converted into motor speed records by applying a flat top moving-window discrete Fourier Transform (window size of 1.6384 s with 0.01 s step) as described previously [52, 62]. The speed recordings are then processed by removing values between -10 and 10 Hz and disregarding -50 and 50 Hz AC frequencies. Remaining data points are median filtered with a moving window of 201 points for Fig. 3, top and middle panel. For Fig. 3 bottom panel, speed recordings were processed as described previously [62].

Acknowledgements

TP, EK, JR and UEPB acknowledge the support from the Office of Naval Research Global and Defense Advanced Research Projects Agency (GRANT12420502). CJL is financially supported by the Ministry of Science and Technology, Republic of China under contract No. MOST-107-2112-M-008-025-MY3. We thank the members of Pilizota and Lo labs, Leonardo

Mancini, Meriem El Karoui, Filippo Menolascina and Vincent Martinez for useful discussions, and Ashley Nord for providing the data from [12] presented in Fig. 5B.

References

[1] H. C. Berg, R. A. Anderson, Bacteria swim by rotating their flagellar filaments, Nature 245 (5425) (1973) 380–382. doi:10.1038/245380a0.

[2] M. Silverman, M. Simon, Flagellar rotation and the mechanism of bacterial motility, Nature 249 (5452) (1974) 73–74. doi:10.1038/249073a0.

[3] H. C. Berg, The rotary motor of bacterial flagella, Annual Review of Biochemistry 72 (1) (2003) 19–54. doi:10.1146/annurev.biochem.72.121801.161737.

[4] Y. Sowa, R. M. Berry, Bacterial flagellar motor, Q. Rev. Biophys. 41 (2) (2008) 103–132. doi:10.1017/S0033583508004691.

[5] J. A. Nirody, Y.-R. Sun, C.-J. Lo, The biophysicist's guide to the bacterial flagellar motor, Adv. Phys. X 2 (2) (2017) 324–343. doi:10.1080/23746149.2017.1289120.

[6] M. Beeby, Motility in the epsilon-proteobacteria, Current Opinion in Microbiology 28 (2015) 115–121. doi:10.1016/j.mib.2015.09.005.

[7] D. Stock, K. Namba, L. K. Lee, Nanorotors and self-assembling macromolecular machines: The torque ring of the bacterial flagellar motor, Current Opinion in Biotechnology 23 (4) (2012) 545–554. doi:10.1016/j.copbio.2012.01.008.

[8] S. Kojima, D. F. Blair, Solubilization and Purification of the MotA/MotB Complex of Escherichia coli, Biochemistry 43 (1) (2004) 26–34. doi:10.1021/bi035405l.

[9] S. W. Reid, M. C. Leake, J. H. Chandler, C.-J. Lo, J. P. Armitage, R. M. Berry, The maximum number of torque-generating units in the flagellar motor of Escherichia coli is at least 11, Proc. Natl. Acad. Sci. U. S. A. 103 (21) (2006) 8066–8071. doi:10.1073/pnas.0509932103.

[10] P. P. Lele, B. G. Hosu, H. C. Berg, Dynamics of mechanosensing in the bacterial flagellar motor, Proc. Natl. Acad. Sci. U. S. A. 110 (29) (2013) 11839–11844. doi:10.1073/pnas.1305885110.

[11] M. J. Tipping, N. J. Delalez, R. Lim, R. M. Berry, J. P. Armitage, Load-dependent assembly of the bacterial flagellar motor, MBio 4 (4) (2013). doi:10.1128/mBio.00551-13.

[12] A. L. Nord, E. Gachon, R. Perez-Carrasco, J. A. Nirody, A. Barducci, R. M. Berry, F. Pedaci, Catch bond drives stator mechanosensitivity in the bacterial flagellar motor, Proc. Natl. Acad. Sci. U. S. A. (2017) 201716002doi:10.1073/pnas.1716002114.

[13] J. C. Deme, S. Johnson, O. Vickery, A. Muellbauer, H. Monkhouse, T. Griffiths, R. H. James, B. C. Berks, J. W. Coulton, P. J. Stansfeld, S. M. Lea, Structures of the stator complex that drives rotation of the bacterial flagellum, preprint, Biochemistry (May 2020). doi:10.1101/2020.05.12.089201.
URL http://biorxiv.org/lookup/doi/10.1101/2020.05.12.089201

[14] M. Santiveri, A. Roa-Eguiara, C. Kühne, N. Wadhwa, H. C. Berg, M. Erhardt, N. M. I. Taylor, Structure and function of stator units of the bacterial flagellar motor, preprint, Biophysics (May 2020). doi:10.1101/2020.05.15.096610.
URL http://biorxiv.org/lookup/doi/10.1101/2020.05.15.096610

[15] Y. Magariyama, S. Sugiyama, K. Muramoto, Y. Maekawa, I. Kawagishi, Y. Imae, S. Kudo, Very fast flagellar rotation, Nature 371 (6500) (1994) 752. doi:10.1038/371752b0.

[16] J. Adler, Chemotaxis in Bacteria, Annual Review of Biochemistry 44 (1) (1975) 341–356. doi:10.1146/annurev.bi.44.070175.002013.

[17] S. M. Block, J. E. Segall, H. C. Berg, Adaptation kinetics in bacterial chemotaxis., J. Bacteriol. 154 (1) (1983) 312–23.

[18] V. Sourjik, N. S. Wingreen, Responding to chemical gradients: Bacterial chemotaxis, Current Opinion in Cell Biology 24 (2) (2012) 262–268. doi:10.1016/j.ceb.2011.11.008.

[19] S. H. Larsen, R. W. Reader, E. N. Kort, W.-W. Tso, J. Adler, Change in direction of flagellar rotation is the basis of the chemotactic response in Escherichia coli, Nature 249 (5452) (1974) 74–77. doi:10.1038/249074a0.

[20] K. K. Mandadapu, J. A. Nirody, R. M. Berry, G. Oster, Mechanics of torque generation in the bacterial flagellar motor, Proc. Natl. Acad. Sci. U. S. A. 112 (32) (2015) E4381–E4389. arXiv:arXiv:1501.02883v1, doi:10.1073/pnas.1501734112.

[21] Y. Magariyama, S. Sugiyama, K. Muramoto, I. Kawagishi, Y. Imae, S. Kudo, Simultaneous measurement of bacterial flagellar rotation rate and swimming speed., Biophysical Journal 69 (1995) 2154–2162. doi:10.1016/S0006-3495(95)80089-5.

[22] Y. Magariyama, S. Sugiyama, S. Kudo, Bacterial swimming speed and rotation rate of bundled flagella, FEMS Microbiology Letters 199 (1) (2001) 125–129. doi:10.1016/S0378-1097(01)00166-5.

[23] H. C. Berg, How to track bacteria, Review of Scientific Instruments 42 (6) (1971) 868–871. doi:10.1063/1.1685246.

[24] L. Xie, T. Altindal, S. Chattopadhyay, X. L. Wu, Bacterial flagellum as a propeller and as a rudder for efficient chemotaxis, Proceedings of the National Academy of Sciences of the United States of America 108 (6) (2011) 2246–2251. doi:10.1073/pnas.1011953108.

[25] J. Schwarz-Linek, J. Arlt, A. Jepson, A. Dawson, T. Vissers, D. Miroli, T. Pilizota, V. A. Martinez, W. C. Poon, Escherichia coli as a model active colloid: A practical introduction, Colloids Surfaces B Biointerfaces 137 (2016) 2–16. arXiv:1506.04562v1, doi:10.1016/j.colsurfb.2015.07.048.

[26] K. Bente, S. Mohammadinejad, M. A. Charsooghi, F. Bachmann, A. Codutti, C. T. Lefèvre, S. Klumpp, D. Faivre, High-speed motility originates from cooperatively pushing and pulling flagella bundles in bilophotrichous bacteria, eLife 9 (2020) 629121. doi:10.7554/eLife.47551.

[27] B. Liu, M. Gulino, M. Morse, J. X. Tang, T. R. Powers, K. S. Breuer, Helical motion of the cell body enhances Caulobacter crescentus motility, Proceedings of the National Academy of Sciences of the United States of America 111 (31) (2014) 11252–11256. doi:10.1073/pnas.1407636111.

[28] K. M. Taute, S. Gude, S. J. Tans, T. S. Shimizu, High-throughput 3D tracking of bacteria on a standard phase contrast microscope, Nature Communications 6 (1) (2015) 8776. doi:10.1038/ncomms9776.

[29] L. Turner, L. Ping, M. Neubauer, H. C. Berg, Visualizing Flagella while Tracking Bacteria, Biophysical Journal 111 (3) (2016) 630–639. doi:10.1016/j.bpj.2016.05.053.

[30] N. Figueroa-Morales, R. Soto, G. Junot, T. Darnige, C. Douarche, V. A. Martinez, A. Lindner, É. Clément, 3D Spatial Exploration by E. coli Echoes Motor Temporal Variability , Physical Review X 10 (2) (2020) 1–12. doi:10.1103/physrevx.10.021004.

[31] T. Darnige, N. Figueroa-Morales, P. Bohec, A. Lindner, E. Clément, Lagrangian 3D tracking of fluorescent microscopic objects in motion, Review of Scientific Instruments 88 (5) (2017). doi:10.1063/1.4982820.

[32] L. G. Wilson, V. A. Martinez, J. Schwarz-Linek, J. Tailleur, G. Bryant, P. N. Pusey, W. C. Poon, Differential dynamic microscopy of bacterial motility, Physical Review Letters 106 (1) (2011) 018101. arXiv:1004.4764, doi:10.1103/PhysRevLett.106.018101.

[33] V. A. Martinez, R. Besseling, O. A. Croze, J. Tailleur, M. Reufer, J. Schwarz-Linek, L. G. Wilson, M. A. Bees, W. C. Poon, Differential dynamic microscopy: A high-throughput method for characterizing the motility of microorganisms, Biophysical Journal 103 (8) (2012) 1637–1647. arXiv:1202.1702, doi:10.1016/j.bpj.2012.08.045.

[34] J. Saragosti, V. Calvez, N. Bournaveas, B. Perthame, A. Buguin, P. Silberzan, Directional persistence of chemotactic bacteria in a traveling concentration wave, Proceedings of the National Academy of Sciences of the United States of America 108 (39) (2011) 16235–16240. doi:10.1073/pnas.1101996108.

[35] M. Bedrossian, M. El-Kholy, D. Neamati, J. Nadeau, A machine learning algorithm for identifying and tracking bacteria in three dimensions using Digital Holographic Microscopy, AIMS Biophysics 5 (1) (2018) 36–49. doi:10.3934/biophy.2018.1.36.

[36] M. J. Schnitzer, Theory of continuum random walks and application to chemotaxis, Physical Review E 48 (4) (1993) 2553–2568. doi:10.1103/PhysRevE.48.2553.

[37] C. Kurzthaler, Y. Zhao, J. Schwartz-Linek, C. Devailly, N. Zhou, J. Arlt, J. D. Huang, W. C. K. Poon, T. Franosch, J. Tailleur, V. A. Martinez, Direct characterization of the run-and-tumble dynamics of swimming bacteria using differential dynamics microscopy, In Preparation.

[38] R. Tecon, J. R. van der Meer, Information from single-cell bacterial biosensors: what is it good for?, Current Opinion in Biotechnology 17 (1) (2006) 4–10. doi:10.1016/j.copbio.2005.11.001.

[39] M. Meister, G. Lowe, H. C. Berg, The proton flux through the bacterial flagellar motor, Cell 49 (5) (1987) 643–650. doi:10.1016/0092-8674(87)90540-X.

[40] M. C. Leake, J. H. Chandler, G. H. Wadhams, F. Bai, R. M. Berry, J. P. Armitage, Stoichiometry and turnover in single, functioning membrane protein complexes., Nature 443 (7109) (2006) 355–358. doi:10.1038/nature05135.

[41] N. Wadhwa, R. Phillips, H. C. Berg, Torque-dependent remodeling of the bacterial flagellar motor, Proceedings of the National Academy of Sciences of the United States of America 116 (24) (2019) 11764–11769. doi:10.1073/pnas.1904577116.

[42] U. Alon, L. Camarena, M. G. Surette, B. A. y. Arcas, Y. Liu, S. Leiber, J. B. Stock, Response regulator output in bacterial chemotaxis, The EMBO Journal 17 (15) (1998) 4238–4248. doi:10.1093/emboj.

[43] J. M. Walter, D. Greenfield, C. Bustamante, J. Liphardt, Light-powering Escherichia coli with proteorhodopsin., Proc. Natl. Acad. Sci. U. S. A. 104 (7) (2007) 2408–12. doi:10.1073/pnas.0611035104.

[44] J. M. Kralj, D. R. Hochbaum, A. D. Douglass, A. E. Cohen, Electrical spiking in Escherichia coli probed with a fluorescent voltage-indicating protein, Science 333 (6040) (2011) 345–348. arXiv:NIHMS150003, doi:10.1126/science.1204763.

[45] C. V. Gabel, H. C. Berg, The speed of the flagellar rotary motor of Escherichia coli varies linearly with protonmotive force., Proc. Natl. Acad. Sci. U. S. A. 100 (15) (2003) 8748–8751. doi:10.1073/pnas.1533395100.

[46] W. Denk, W. W. Webb, Optical measurement of picometer displacements of transparent microscopic objects., Appl. Opt. 29 (16) (1990) 2382–2391. doi:10.1364/AO.29.002382.

[47] K. Svoboda, C. F. Schmidt, B. J. Schnapp, S. M. Block, Direct observation of kinesin stepping by optical trapping interferometry, Nature 365 (6448) (1993) 721–727. doi:10.1038/365721a0.

[48] W. S. Ryu, R. M. Berry, H. C. Berg, Torque-generating units of the flagellar motor of Escherichia coli have a high duty ratio, Nature 403 (6768) (2000) 444–447. doi:10.1038/35000233.

[49] H. C. Berg, L. Turner, Torque generated by the flagellar motor of Escherichia coli, Biophys. J. 65 (5) (1993) 2201–16. doi:10.1016/S0006-3495(93)81278-5.

[50] X. Chen, H. C. Berg, Torque-speed relationship of the flagellar rotary motor of Escherichia coli, Biophysical Journal 78 (2) (2000) 1036–1041. doi:10.1016/S0006-3495(00)76662-8.

[51] J. Rosko, Osmotaxis in Escherichia coli, Ph.D. thesis, The Edinburgh University (2017).
URL `http://hdl.handle.net/1842/28947`

[52] E. Krasnopeeva, C.-J. Lo, T. Pilizota, Single-cell bacterial electrophysiology reveals mechanisms of stress-induced damage, Biophysical Journal 116 (12) (2019) 2390–2399. doi:10.1016/j.bpj.2019.04.039.

[53] W. Pfeffer, Über chemotaktische bewegungen von bacterien, flagellaten, und volvocineen, Untersuchungen aus dem Botanischen Institut in Tübingen (2) (1888) 582–661.

[54] J. Adler, A Method for Measuring Chemotaxis and Use of the Method to Determine Optimum Conditions for Chemotaxis by Escherichia coli, Journal of General Microbiology 74 (1) (1973) 77–91. doi:10.1099/00221287-74-1-77.

[55] W.-W. Tso, J. Adler, Negative chemotaxis in escherichia coli, Journal of Bacteriology 118 (2) (1974) 560–576. doi:10.1128/JB.118.2.560-576.1974.

[56] G. Kuwajima, Construction of a minimum-size functional flagellin of Escherichia coli, J. Bacteriol. 170 (7) (1988) 3305–3309. doi:10.1128/jb.170.7.3305-3309.1988.

[57] D. C. Fung, H. C. Berg, Powering the flagellar motor of Escherichia coli with an external voltage source, Nature 375 (6534) (1995) 809–812. doi:10.1038/375809a0.

[58] C. Lo, Y. Sowa, T. Pilizota, R. M. Berry, Mechanism and kinetics of a sodium-driven bacterial flagellar motor, Proc. Natl. Acad. Sci. U. S. A. 110 (28) (2013) E2544–E2551. doi:10.1073/pnas.1301664110.

[59] J. Yuan, H. C. Berg, Resurrection of the flagellar rotary motor near zero load., Proceedings of the National Academy of Sciences of the United States of America 105 (4) (2008) 1182–5. doi:10.1073/pnas.0711539105.

[60] S. Nakamura, Y. Hanaizumi, Y. V. Morimoto, Y. Inoue, M. Erhardt, T. Minamino, K. Namba, Direct observation of speed fluctuations of flagellar motor rotation at extremely low load close to zero, Molecular Microbiology 113 (4) (2020) 755–765. doi:10.1111/mmi.14440.

[61] M. T. Brown, B. C. Steel, C. Silvestrin, D. A. Wilkinson, N. J. Delalez, C. N. Lumb, B. Obara, J. P. Armitage, R. M. Berry, Flagellar hook flexibility is essential for bundle formation in swimming escherichia coli cells, Journal of Bacteriology 194 (13) (2012) 3495–3501. doi:10.1128/JB.00209-12.

[62] J. Rosko, V. Martinez, W. Poon, T. Pilizota, Osmotaxis in Escherichia coli through changes in motor speed, Proc. Natl. Acad. Sci. U. S. A. 114 (38) (2017) E7969–E7976. arXiv:1703.03926, doi:10.1073/pnas.1620945114.

[63] F. Bai, R. W. Branch, D. V. Nicolau, T. Pilizota, B. C. Steel, P. K. Maini, R. M. Berry, Conformational spread as a mechanism for cooperativity in the bacterial flagellar switch, Science 327 (5966) (2010) 685–689. doi:10.1126/science.1182105.

[64] L. Mancini, G. Terradot, T. Tian, Y. Y. Pu, Y. Li, C. J. Lo, F. Bai, T. Pilizota, A General Workflow for Characterization of Nernstian Dyes and Their Effects on Bacterial Physiology, Biophysical Journal (2019). doi:10.1016/j.bpj.2019.10.030.

[65] T. Pilizota, T. Bilyard, F. Bai, M. Futai, H. Hosokawa, R. M. Berry, A programmable optical angle clamp for rotary molecular motors, Biophys. J. 93 (1) (2007) 264–275. doi:10.1529/biophysj.106.091074.

[66] T. J. Zajdel, A. N. Walczak, D. Sengupta, V. Tieu, B. Rad, M. M. Maharbiz, Towards a biohybrid sensing platform built on impedance-based bacterial flagellar motor tachometry, in: 2017 IEEE Biomedical Circuits and Systems Conference (BioCAS), IEEE, Torino, 2017, pp. 1–4. doi:10.1109/BIOCAS.2017.8325135.

[67] T. Zajdel, Electronic Interfaces for Bacteria-Based Biosensing, Ph.D. thesis, University of California at Berkeley (2018).

[68] J. Adler, Chemoreceptors in bacteria, Science 166 (3913) (1969) 1588–1597. doi:10.1126/science.166.3913.1588.

[69] W. Pfeffer, Locomotorische Richtungsbewegungen durch chemische Reize., Vnters. Bot. Inst. Tiibinyen 1: (1884) 363–482.

[70] H. C. Berg, Chemotaxis in bacteria, Annual Review of Biophysics and Bioengineering 4 (1) (1975) 119–136. doi:10.1146/annurev.bb.04.060175.001003.

[71] H. Berg, L. Turner, Chemotaxis of bacteria in glass capillary arrays. Escherichia coli, motility, microchannel plate, and light scattering, Biophysical Journal 58 (4) (1990) 919–930. doi:10.1016/S0006-3495(90)82436-X.

[72] P. D. Frymier, R. M. Ford, H. C. Berg, P. T. Cummings, Three-dimensional tracking of motile bacteria near a solid planar surface.,

760 Proceedings of the National Academy of Sciences 92 (13) (1995) 6195–
761 6199. doi:10.1073/pnas.92.13.6195.

762 [73] L. Turner, W. S. Ryu, H. C. Berg, Real-time imaging of fluo-
763 rescent flagellar filaments, J. Bacteriol. 182 (10) (2000) 2793–2801.
764 doi:10.1128/JB.182.10.2793-2801.2000.

765 [74] G. H. Wadhams, J. P. Armitage, Making sense of it all: bacterial
766 chemotaxis, Nature Reviews Molecular Cell Biology 5 (12) (2004) 1024–
767 1037. doi:10.1038/nrm1524.

768 [75] M. Welch, K. Oosawa, S. Aizawa, M. Eisenbach, Phosphorylation-
769 dependent binding of a signal molecule to the flagellar switch of bacte-
770 ria., Proceedings of the National Academy of Sciences 90 (19) (1993)
771 8787–8791. doi:10.1073/pnas.90.19.8787.

772 [76] R. Barak, M. Eisenbach, Correlation between phosphorylation of the
773 chemotaxis protein CheY and its activity at the flagellar motor, Bio-
774 chemistry 31 (6) (1992) 1821–1826. doi:10.1021/bi00121a034.

775 [77] T. Minamino, M. Kinoshita, K. Namba, Directional switching mech-
776 anism of the bacterial flagellar motor, Computational and Structural
777 Biotechnology Journal 17 (2019) 1075–1081.

778 [78] A. J. Wolfe, M. P. Conley, T. J. Kramer, H. C. Berg, Reconstitution
779 of signaling in bacterial chemotaxis., Journal of Bacteriology 169 (5)
780 (1987) 1878–1885. doi:10.1128/JB.169.5.1878-1885.1987.

781 [79] Ortega, I. B. Zhulin, T. Krell, Sensory Repertoire of Bacterial
782 Chemoreceptors, Microbiology and Molecular Biology Reviews 81 (4)
783 (2017) e00033–17, e00033–17. doi:10.1128/MMBR.00033-17.

784 [80] D. M. Miller, J. S. Olson, J. W. Pflugrath, F. A. Quiocho, Rates of lig-
785 and binding to periplasmic proteins involved in bacterial transport and
786 chemotaxis., Journal of Biological Chemistry 258 (22) (1983) 13665–
787 13672.

788 [81] Y. Meir, V. Jakovljevic, O. Oleksiuk, V. Sourjik, N. S. Wingreen, Pre-
789 cision and kinetics of adaptation in bacterial chemotaxis, Biophysical
790 Journal 99 (9) (2010) 2766–2774. doi:10.1016/j.bpj.2010.08.051.

[82] A. K. Krembel, S. Neumann, V. Sourjik, Universal Response-Adaptation Relation in Bacterial Chemotaxis, Journal of Bacteriology 197 (2) (2015) 307–313. doi:10.1128/JB.02171-14.

[83] R. Mesibov, J. Adler, Chemotaxis toward amino acids in escherichia coli, Journal of Bacteriology 112 (1) (1972) 315–326. doi:10.1128/JB.112.1.315-326.1972.

[84] J. Adler, G. L. Hazelbauer, M. M. Dahl, Chemotaxis toward sugars in escherichia coli, Journal of Bacteriology 115 (3) (1973) 824–847. doi:10.1128/JB.115.3.824-847.1973.

[85] M. Hegde, D. L. Englert, S. Schrock, W. B. Cohn, C. Vogt, T. K. Wood, M. D. Manson, A. Jayaraman, Chemotaxis to the quorum-sensing signal ai-2 requires the tsr chemoreceptor and the periplasmic lsrb ai-2-binding protein, Journal of Bacteriology 193 (3) (2011) 768–773. doi:10.1128/JB.01196-10.

[86] L. Laganenka, R. Colin, V. Sourjik, Chemotaxis towards autoinducer 2 mediates autoaggregation in Escherichia coli, Nature Communications 7 (1) (2016) 12984. doi:10.1038/ncomms12984.

[87] R. W. Reader, W. W. Tso, M. S. Springer, M. F. Goy, J. Adler, Pleiotropic aspartate taxis and serine taxis mutants of Escherichia coli., Journal of general microbiology 111 (2) (1979) 363–74. doi:10.1099/00221287-111-2-363.

[88] S. Bi, A. M. Pollard, Y. Yang, F. Jin, V. Sourjik, Engineering Hybrid Chemotaxis Receptors in Bacteria, ACS Synthetic Biology 5 (9) (2016) 989–1001. doi:10.1021/acssynbio.6b00053.

[89] K. Jung, F. Fabiani, E. Hoyer, J. Lassak, Bacterial transmembrane signalling systems and their engineering for biosensing, Open Biology 8 (4) (2018) 180023. doi:10.1098/rsob.180023.

[90] R. A. Luu, R. A. Schomer, C. N. Brunton, R. Truong, A. P. Ta, W. A. Tan, J. V. Parales, Y.-J. Wang, Y.-W. Huo, S.-J. Liu, J. L. Ditty, V. Stewart, R. E. Parales, Hybrid two-component sensors for identification of bacterial chemoreceptor function, Applied and Environmental Microbiology 85 (22) (2019) e01626–19, /aem/85/22/AEM.01626–19.atom. doi:10.1128/AEM.01626-19.

[91] H.-J. Chang, P. Mayonove, A. Zavala, A. De Visch, P. Minard, M. Cohen-Gonsaud, J. Bonnet, A Modular Receptor Platform To Expand the Sensing Repertoire of Bacteria, ACS Synthetic Biology 7 (1) (2018) 166–175. doi:10.1021/acssynbio.7b00266.

[92] H.-J. Chang, J. Bonnet, Synthetic receptors to understand and control cellular functions, in: Methods in Enzymology, Vol. 633, Elsevier, 2020, pp. 143–167. doi:10.1016/bs.mie.2019.11.011.

[93] N. Vladimirov, V. Sourjik, Chemotaxis: how bacteria use memory, Biological Chemistry 390 (11) (2009) 1097–1104. doi:10.1515/BC.2009.130.

[94] CheZ-Mediated Dephosphorylation of the Escherichia coli Chemotaxis Response Regulator CheY: Role for CheY Glutamate 89 185. doi:10.1128/JB.185.5.1495-1502.2003.

[95] M. J. Tindall, E. A. Gaffney, P. K. Maini, J. P. Armitage, Theoretical insights into bacterial chemotaxis: Theoretical bacterial chemotaxis, Wiley Interdisciplinary Reviews: Systems Biology and Medicine 4 (3) (2012) 247–259. doi:10.1002/wsbm.1168.

[96] M. V. Airola, N. Sukomon, D. Samanta, P. P. Borbat, J. H. Freed, K. J. Watts, B. R. Crane, HAMP Domain Conformers That Propagate Opposite Signals in Bacterial Chemoreceptors, PLoS Biology 11 (2) (2013) e1001479. doi:10.1371/journal.pbio.1001479.

[97] S. L. Porter, M. A. J. Roberts, C. S. Manning, J. P. Armitage, A bifunctional kinase-phosphatase in bacterial chemotaxis, Proceedings of the National Academy of Sciences 105 (47) (2008) 18531–18536. doi:10.1073/pnas.0808010105.

[98] S. Yagur-Kroll, C. Lalush, R. Rosen, N. Bachar, Y. Moskovitz, S. Belkin, Escherichia coli bioreporters for the detection of 2,4-dinitrotoluene and 2,4,6-trinitrotoluene, Applied Microbiology and Biotechnology 98 (2) (2014) 885–895. doi:10.1007/s00253-013-4888-8.

[99] C. Roggo, C. Picioreanu, X. Richard, C. Mazza, H. van Lintel, J. R. van der Meer, Quantitative chemical biosensing by bacterial chemotaxis in microfluidic chips: Chemotaxis-microfluidic biosensor, Environmental Microbiology 20 (1) (2018) 241–258. doi:10.1111/1462-2920.13982.

[100] C. Lin, Q.-X. Zhang, Y.-C. Yeh, Development of a whole-cell biosensor for the determination of tyrosine in urine for point-of-care diagnostics, Analytical Methods 11 (10) (2019) 1400–1404. doi:10.1039/C9AY00070D.

[101] X. Wan, F. Volpetti, E. Petrova, C. French, S. J. Maerkl, B. Wang, Cascaded amplifying circuits enable ultrasensitive cellular sensors for toxic metals, Nature Chemical Biology 15 (5) (2019) 540–548. doi:10.1038/s41589-019-0244-3.

[102] M. Hicks, T. T. Bachmann, B. Wang, Synthetic Biology Enables Programmable Cell-Based Biosensors, ChemPhysChem 21 (2) (2020) 132–144. doi:10.1002/cphc.201900739.

[103] B. E. Scharf, K. A. Fahrner, L. Turner, H. C. Berg, Control of direction of flagellar rotation in bacterialchemotaxis, Proc. Natl. Acad. Sci. U. S. A. 95 (1) (1998).

[104] S. H. Larsen, J. Adler, J. J. Gargus, R. W. Hogg, Chemomechanical coupling without ATP: the source of energy for motility and chemotaxis in bacteria., Proc. Natl. Acad. Sci. U. S. A. 71 (4) (1974) 1239–1243. doi:10.1073/pnas.71.4.1239.

[105] P. Mitchell, Coupling of phosphorylation to electron and hydrogen transfer by a chemi-osmotic type of mechanism, Nature 191 (4784) (1961) 144–148. doi:10.1038/191144a0.

[106] D. G. Nicholls, S. J. Ferguson, Bioenergetics 2, Academic Press, 1992. doi:10.1016/B978-0-12-518124-2.50006-0.

[107] B. Martinac, M. Buechner, A. H. Delcour, J. Adler, C. Kung, Pressure-sensitive ion channel in Escherichia coli., Proc. Natl. Acad. Sci. U. S. A. 84 (8) (1987) 2297–2301. doi:10.1073/pnas.84.8.2297.

[108] J. Benarroch, M. Asally, The microbiologist's guide to membrane potential dynamics, Trends in Microbiology 28 (01 2020). doi:10.1016/j.tim.2019.12.008.

[109] Z. Schofiel, G. Meloni, P. Tran, C. Zerfass, G. Sena, Y. Hayashi, M. Grant, S. A. Contera, S. Minteer, M. Kim, A. Prindle, P. Rocha, M. B. A. Djamgoz, T. Pilizota, P. R. Unwin, M. Asally, O. S. Soyer,

Bioelectrical understanding and engineering of cell biology, Journal of the Royal Society Interface (In Press).

[110] Y. Asai, T. Yakushi, I. Kawagishi, M. Homma, Ion-coupling determinants of na+-driven and h+-driven flagellar motors, Journal of Molecular Biology 327 (2) (2003) 453–463. doi:10.1016/S0022-2836(03)00096-2.

[111] Y. Sowa, M. Homma, A. Ishijima, R. M. Berry, Hybrid-fuel bacterial flagellar motors in *Escherichia coli*, Proceedings of the National Academy of Sciences 111 (9) (2014) 3436–3441. doi:10.1073/pnas.1317741111.

[112] J. Z. Liu, M. Dapice, S. Khan, Ion selectivity of the Vibrio alginolyticus flagellar motor, Journal of Bacteriology 172 (9) (1990) 5236–5244. doi:10.1128/jb.172.9.5236-5244.1990.

[113] N. Terahara, M. Sano, M. Ito, A Bacillus Flagellar Motor That Can Use Both Na+ and K+ as a Coupling Ion Is Converted by a Single Mutation to Use Only Na+, PLoS ONE 7 (9) (2012) e46248. doi:10.1371/journal.pone.0046248.

[114] S. M. Block, H. C. Berg, Successive incorporation of force-generating units in the bacterial rotary motor, Nature 309 (5967) (1984) 470–472. doi:10.1038/309470a0.

[115] G. A. O'Toole, G. C. Wong, Sensational biofilms: surface sensing in bacteria, Current Opinion in Microbiology 30 (2016) 139–146. doi:10.1016/j.mib.2016.02.004.

[116] V. D. Gordon, L. Wang, Bacterial mechanosensing: the force will be with you, always, Journal of Cell Science 132 (7) (2019) jcs227694. doi:10.1242/jcs.227694.

[117] R. Chawla, R. Gupta, T. P. Lele, P. P. Lele, A skeptic's guide to bacterial mechanosensing, Journal of Molecular Biology 432 (2) (2020) 523–533. doi:10.1016/j.jmb.2019.09.004.

[118] L. McCarter, M. Hilmen, M. Silverman, Flagellar dynamometer controls swarmer cell differentiation of V. parahaemolyticus, Cell 54 (3) (1988) 345–351. doi:10.1016/0092-8674(88)90197-3.

[119] L. S. Cairns, V. L. Marlow, E. Bissett, A. Ostrowski, N. R. Stanley-Wall, A mechanical signal transmitted by the flagellum controls signalling in Bacillus subtilis, Molecular Microbiology 90 (1) (2013) 6–21. doi:10.1111/mmi.12342.

[120] S. B. Guttenplan, D. B. Kearns, Regulation of flagellar motility during biofilm formation, FEMS Microbiology Reviews 37 (6) (2013) 849–871. doi:10.1111/1574-6976.12018.

[121] L. Laganenka, M. E. López, R. Colin, V. Sourjik, Flagellum-Mediated Mechanosensing and RflP Control Motility State of Pathogenic Escherichia coli, mBio 11 (2) (mar 2020). doi:10.1128/mBio.02269-19.

[122] C. S. Barker, B. M. Prüß, P. Matsumura, Increased motility of Escherichia coli by insertion sequence element integration into the regulatory region of the flhD operon, J. Bacteriol. 186 (22) (2004) 7529–7537. doi:10.1128/JB.186.22.7529-7537.2004.

[123] J. Cremer, T. Honda, Y. Tang, J. Wong-Ng, M. Vergassola, T. Hwa, Chemotaxis as a navigation strategy to boost range expansion, Nature 575 (7784) (2019) 658–663. doi:10.1038/s41586-019-1733-y.

[124] J. Adler, B. Templeton, The effect of environmental conditions on the motility of Escherichia coli., Journal of general microbiology 46 (2) (1967) 175–184. doi:10.1099/00221287-46-2-175.

[125] C. Li, C. J. Louise, W. Shi, J. Adler, Adverse conditions which cause lack of flagella in Escherichia coli., Journal of Bacteriology 175 (8) (1993) 2229–2235.

[126] C. D. Amsler, M. Cho, P. Matsumura, Multiple factors underlying the maximum motility of Escherichia coli as cultures enter post-exponential growth, J. Bacteriol. 175 (19) (1993) 6238–6244. doi:10.1128/jb.175.19.6238-6244.1993.

[127] A. Boehm, M. Kaiser, H. Li, C. Spangler, C. A. Kasper, M. Ackermann, V. Kaever, V. Sourjik, V. Roth, U. Jenal, Second Messenger-Mediated Adjustment of Bacterial Swimming Velocity, Cell 141 (1) (2010) 107–116. doi:10.1016/j.cell.2010.01.018.

[128] R. Belas, Biofilms, flagella, and mechanosensing of surfaces by bacteria, Trends in Microbiology 22 (9) (2014) 517–527. doi:10.1016/j.tim.2014.05.002.

[129] L. M. Maurer, E. Yohannes, S. S. Bondurant, M. Radmacher, J. L. Slonczewski, pH Regulates Genes for Flagellar Motility, Catabolism, and Oxidative Stress in Escherichia coli K-12, Journal of Bacteriology 187 (1) (2005) 304–319. doi:10.1128/JB.187.1.304-319.2005.

[130] K. Paul, V. Nieto, W. C. Carlquist, D. F. Blair, R. M. Harshey, The c-di-GMP Binding Protein YcgR Controls Flagellar Motor Direction and Speed to Affect Chemotaxis by a "Backstop Brake" Mechanism, Mol. Cell 38 (1) (2010) 128–139. doi:10.1016/j.molcel.2010.03.001.

[131] S. H. Collins, W. A. Hamilton, Magnitude of the protonmotive force in respiring Staphylococcus aureus and Escherichia coli, J. Bacteriol. 126 (3) (1976) 1224–1231.

[132] Q. H. Tran, G. Unden, Changes in the proton potential and the cellular energetics of Escherichia coli during growth by aerobic and anaerobic respiration or by fermentation, Eur. J. Biochem. 251 (1-2) (1998) 538–543. doi:10.1046/j.1432-1327.1998.2510538.x.

[133] Y. Sowa, H. Hotta, M. Homma, A. Ishijima, Torque-speed relationship of the Na+-driven flagellar motor of Vibrio alginolyticus, J. Mol. Biol. 327 (5) (2003) 1043–1051. doi:10.1016/S0022-2836(03)00176-1.

[134] M. J. Tipping, B. C. Steel, N. J. Delalez, R. M. Berry, J. P. Armitage, Quantification of flagellar motor stator dynamics through in vivo proton-motive force control, Mol. Microbiol. 87 (2) (2013) 338–347. doi:10.1111/mmi.12098.

[135] S. Ahmed, I. R. Booth, The use of valinomycin, nigericin and trichlorocarbanilide in control of the protonmotive force in Escherichia coli cells, Biochemical Journal 212 (1) (1983) 105–112. doi:10.1042/bj2120105.

[136] J. Yuan, K. A. Fahrner, L. Turner, H. C. Berg, Asymmetry in the clockwise and counterclockwise rotation of the bacterial flagellar motor, Proceedings of the National Academy of Sciences of the United States of America 107 (29) (2010) 12846–12849. doi:10.1073/pnas.1007333107.

[137] Y. Sowa, A. D. Rowe, M. C. Leake, T. Yakushi, M. Homma, A. Ishijima, R. M. Berry, Direct observation of steps in rotation of the bacterial flagellar motor., Nature 437 (7060) (2005) 916–919. doi:10.1038/nature04003.

[138] S. Nakamura, N. Kami-ike, J.-i. P. Yokota, T. Minamino, K. Namba, Evidence for symmetry in the elementary process of bidirectional torque generation by the bacterial flagellar motor., Proceedings of the National Academy of Sciences of the United States of America 107 (2010) 17616–17620. doi:10.1073/pnas.1007448107.

[139] T. Baba, T. Ara, M. Hasegawa, Y. Takai, Y. Okumura, M. Baba, K. A. Datsenko, M. Tomita, B. L. Wanner, H. Mori, Construction of *Escherichia coli* K-12 in-frame, single-gene knockout mutants: the Keio collection, Molecular Systems Biology 2 (1) (Jan. 2006). doi:10.1038/msb4100050.

[140] L. C. Thomason, N. Costantino, D. L. Court, *e. Coli* genome manipulation by p1 transduction, in: F. M. Ausubel, R. Brent, R. E. Kingston, D. D. Moore, J. Seidman, J. A. Smith, K. Struhl (Eds.), Current Protocols in Molecular Biology, John Wiley & Sons, Inc., Hoboken, NJ, USA, 2007, pp. 1.17.1–1.17.8. doi:10.1002/0471142727.mb0117s79. URL `http://doi.wiley.com/10.1002/0471142727.mb0117s79`

[141] A. Saragliadis, T. Trunk, J. C. Leo, Producing gene deletions in escherichia coli by p1 transduction with excisable antibiotic resistance cassettes, Journal of Visualized Experiments (139) (2018) 58267. doi:10.3791/58267.

[142] T. Pilizota, J. W. Shaevitz, Fast, multiphase volume adaptation to hyperosmotic shock by Escherichia coli, PLoS One 7 (4) (2012) e35205. doi:10.1371/journal.pone.0035205.